J Electroceram (2007) 18:25–31
DOI 10.1007/s10832-007-9004-y

Dielectric properties of Zn- and/or Nb-substituted $Pb[(Mg_{1/3}Ta_{2/3}),Ti]O_3$ ceramics

Jee-Su Kim · Dong-Hwan Suh · Nam-Kyoung Kim

Received: 19 August 2004 / Accepted: 23 May 2006 / Published online: 22 February 2007

Abstract Ceramic powders of $Pb[(Mg_{1/3}Ta_{2/3}),Ti]O_3$, with the octahedral components substituted separately as well as simultaneously by Zn and Nb, were synthesized by a two-step B-site precursor method. Prepared powders were examined by X-ray diffraction (XRD) to monitor the phase developments and also to determine the crystallographic aspects. The weak-field low-frequency dielectric constant and loss values of the sintered specimens were determined. Temperature-dependent dielectric constant values were further analyzed in terms of diffuseness/sharpness in the phase transition modes. The internal microstructures of the ceramics were examined by scanning electron microscopy (SEM).

Keywords PMT · PMT-PT · Perovskite · Ceramics · Dielectric property

1 Introduction

Lead magnesium tantalate $Pb(Mg_{1/3}Ta_{2/3})O_3$ (PMT) is a complex-perovskite ferroelectric relaxor, that exhibits frequency-dependent dielectric dispersion behavior with diffuse modes (broadened dielectric maxima) in the phase transition [1–3]. When compared with the prototype relaxors $Pb(Mg_{1/3}Nb_{2/3})O_3$ and $Pb(Zn_{1/3}Nb_{2/3})O_3$ (PMN and PZN, respectively), however, PMT has not been studied as much. The lack of interest in PMT so far can be attributed (at least in part) to the dielectric maximum temperature of −98°C, which is rather low for practical applications [1, 4–7]. Meanwhile, $Pb(Zn_{1/3}Ta_{2/3})O_3$ (PZT) has not been synthesized to a perovskite structure yet [6–11] in spite of its stoichiometry identical to those of complex-perovskite PMT, PMN, and PZN. It should be noted that PZT in the present paper does not stand for piezoelectric $Pb(Zr,Ti)O_3$, but instead for a Zn analog of PMT (or a Ta analog of PZN). Lead titanate $PbTiO_3$ (PT) is one of the earliest-known tetragonal perovskites with a very high Curie temperature (490°C) and rather sharp phase transition modes.

Several studies on the dielectric properties of the $Pb[(Mg_{1/3}Ta_{2/3}),Ti]O_3$ (i.e., PMT-PT) pseudobinary system have been reported to date, especially near the morphotropic phase boundaries [5, 12, 13]. However, sinterability of stoichiometric PT powder compacts is known to be rather poor owing to the development of microcracks (induced from the large crystallographic anisotropy of c/a= 1.065, ICDD No. 6-452) on passing through the phase transition temperature during cooling. In the present study, therefore, Zn and Nb as well as the Zn-Nb complex were introduced into the octahedral lattice sites of the PMT-PT system and resultant properties were investigated. The main objectives of the study include the examination of the role of the substituent cation species (introduced either separately or simultaneously) on the dielectric properties of the ceramics as well as on the sinterability (especially at PT-rich compositions). It is also expected that reduction of the wide range of dielectric maximum temperatures can be achieved, as the temperatures of the three substituent species of PMN, PZN, and hypothetical perovskite PZT (extrapolated values [7, 10, 11]) are positioned between those of the end components, PMT and PT.

Thus far, pyrochlore phase(s) have been reported to develop occasionally in certain $Pb\left(B'_{1/3}B''_{2/3}\right)O_3$ compositions, including PZT [6–11] and PZN [6, 8, 14–17], during

J.-S. Kim · D.-H. Suh · N.-K. Kim (✉)
Department of Inorganic Materials Engineering,
Kyungpook National University, Daegu 702-701, South Korea
e-mail: nkkim@knu.ac.kr

the perovskite formation by solid-state reactions under ambient pressure. It is also well known that presence of the parasitic pyrochlore(s) in the perovskite matrix, even in small quantities, significantly degrades the dielectric properties [8, 18, 19]. Therefore, a two-step route of the B-site precursor method [20, 21] (a more comprehensive concept for the widely adopted columbite process [22, 23]) was employed in the present study in order to suppress the formation of unwanted pyrochlore(s) and thereby to improve the dielectric properties.

2 Experimental procedure

The three systems under investigation are (0.8-*x*)PMT-*x*PT-0.2PZT, (0.8-*y*)PMT-*y*PT-0.2PMN, and (0.8-*z*)PMT-*z*PT-0.2PZN (Systems I, II, and III, respectively). Starting materials were high-purity oxide chemicals of PbO (99.5% purity), MgO (99.9%), ZnO (99.8%), Ta_2O_5 (99.9%), Nb_2O_5 (99.9%), and TiO_2 (99.9%). In order to maintain the complex stoichiometries as close to the nominal values as possible, the moisture contents of the raw chemicals and of the separately synthesized B-site precursor powders were measured and introduced into the batch calculations.

B-site precursor powders of the three systems were synthesized by wet-milling, drying, and reacting the powder mixtures at 1,050–1,250°C (depending on compositions) for 2 h in air. The products were milled, dried, and calcined again at identical conditions to promote phase formation. After the addition of PbO in stoichiometric proportions, the powders were reacted at 800–850 and 800–950°C for 2 h each with intermediate milling and drying steps. Thus-prepared powders were examined by XRD to identify the developed phases and also to investigate the crystallographic aspects. The powders (with 2 wt% aqueous solution of a polyvinyl alcohol binder) were isostatically formed into pellet-type specimens. The preforms were fired at 1,100–1,300°C for 1 h (soaking time) in a multiple-enclosure inverted-crucible setup [16] to minimize lead loss during exposure to high temperatures. Sintered samples were ground/polished to attain parallel surfaces, over which gold was sputtered for electrical contacts. The low-frequency weak-field (1–1,000 kHz, ~1 V_{rms}/mm) dielectric constant and loss values were determined from capacitance values measured on cooling using an impedance analyzer. The samples were then fractured, gold-coated, and the internal microstructures were examined by SEM.

3 Results and discussion

XRD results of the precursor compositions are compared in Fig. 1. In the Zn-substituted case of (0.8-*x*)$(Mg_{1/3}Ta_{2/3})$

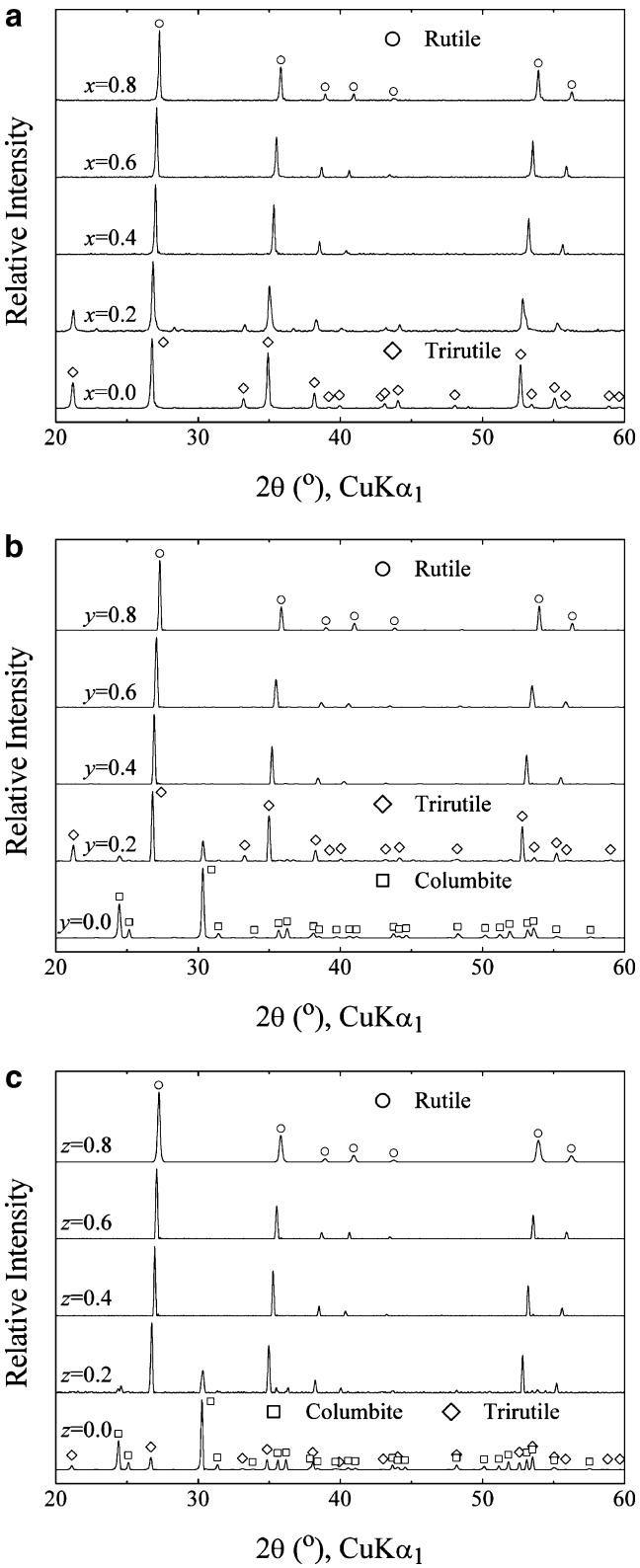

Fig. 1 X-ray diffraction results of the systems **a** (0.8-*x*)$(Mg_{1/3}Ta_{2/3})O_2$-*x*TiO_2-0.2$(Zn_{1/3}Ta_{2/3})O_2$, **b** (0.8-*y*)$(Mg_{1/3}Ta_{2/3})O_2$-*y*TiO_2-0.2$(Mg_{1/3}Nb_{2/3})O_2$, and **c** (0.8-*z*)$(Mg_{1/3}Ta_{2/3})O_2$-*z*TiO_2-0.2$(Zn_{1/3}Nb_{2/3})O_2$

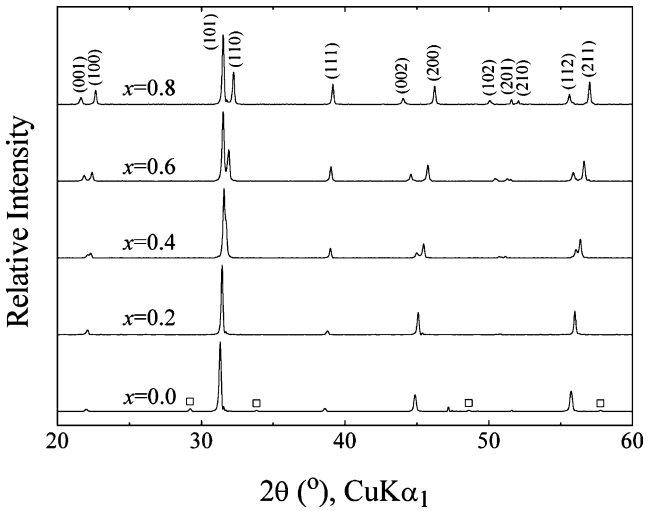

Fig. 2 XRD spectra of (0.8-*x*)PMT-*x*PT-0.2PZT (System I). (*hkl*) perovskite, (*empty square*) pyrochlore

O_2-$x$$TiO_2$-0.2($Zn_{1/3}Ta_{2/3}$)$O_2$, Fig. 1a, only a trirutile structure ($MgTa_2O_6$, ICDD No. 32-631) formed at x=0.0 of 0.8($Mg_{1/3}Ta_{2/3}$)O_2-0.2($Zn_{1/3}Ta_{2/3}$)O_2, indicating that the 20 mol% component of ($Zn_{1/3}Ta_{2/3}$)O_2 had structurally assimilated to the trirutile matrix. At the opposite end (x=0.8) of 0.2($Zn_{1/3}Ta_{2/3}$)O_2-0.8TiO_2, which can be compositionally partitioned as 0.4[($Zn_{1/3}Ta_{2/3}$)$_{1/2}$$Ti_{1/2}$]$O_2$+0.6$TiO_2$, however, only a rutile structure was identified. The observed rutile structure, of course, could be neither solely of TiO_2 nor of [($Zn_{1/3}Ta_{2/3}$)$_{1/2}$$Ti_{1/2}$]$O_2$ (ICDD Nos. 21–1276 and 39–292, respectively), but rather is a solid solution formed between the two. Close examination on the angular positions of the diffraction peaks confirmed the conclusion. The structure of the rutile solid solution (x=0.8) persisted down to x=0.4, whereas two structures of trirutile and rutile were observed to coexist at x=0.2 as 0.6($Mg_{1/3}Ta_{2/3}$)O_2+0.4[($Zn_{1/3}Ta_{2/3}$)$_{1/2}$$Ti_{1/2}$]$O_2$. It was also observable that the angular positions of the trirutile and rutile were slightly higher and lower, respectively, than the anticipated values (calculated from the ICDD data). The systematic counter-shifts indicate that the two components had actually dissolved into each other, but only partially. Such compositional dissolution to limited extents can be explained by the structural dissimilarity and, to a lesser degree, also by the difference in the effective ionic radii (weight-averaged values) of $Mg_{1/3}Ta_{2/3}$ and ($Zn_{1/3}Ta_{2/3}$)$_{1/2}$$Ti_{1/2}$: 0.0667 and 0.0639 nm [24].

In the Nb-substituted case of (0.8-y)($Mg_{1/3}Ta_{2/3}$)O_2-$y$$TiO_2$-0.2($Mg_{1/3}Nb_{2/3}$)$O_2$, Fig. 1b, only a columbite structure (based on $MgNb_2O_6$, ICDD No. 33–875) was identified at y=0.0 of 0.8($Mg_{1/3}Ta_{2/3}$)O_2-0.2($Mg_{1/3}Nb_{2/3}$)O_2. Therefore, it is quite interesting to note that the 80 mol% component of ($Mg_{1/3}Ta_{2/3}$)O_2 (trirutile structure) had somehow assimilated structurally to the ($Mg_{1/3}Nb_{2/3}$)O_2 component (20 mol%) to form the columbite solid solution. In contrast, a rutile solid solution was solely detectable at $y\geq$ 0.4, similar to the results of Fig. 1a. Meanwhile, trirutile and columbite structures were observed to coexist at y=0.2. The results in the Zn/Nb-cosubstituted case of (0.8-z)($Mg_{1/3}Ta_{2/3}$)O_2-$z$$TiO_2$-0.2($Zn_{1/3}Nb_{2/3}$)$O_2$, Fig. 1c, were very similar to those of Fig. 1a and b in that only a rutile solid solution developed at $z\geq$0.4. At PMT-rich compositions, however, the columbite and trirutile structures coexisted at z=0.0, whereas both structures of rutile and columbite were identified at z= 0.2. Therefore, the trirutile peaks, present at x=0.0 and 0.2 in the Zn-substituted system, were detected only at y=0.2 and z=0.0 in the Nb-substituted and Zn/Nb-cosubstituted cases.

The X-ray diffractograms of System I, (0.8-x)PMT-xPT-0.2PZT, are displayed in Fig. 2. All of the diffraction peaks were identified as perovskite, except for a negligible fraction of pyrochlore (*empty square*) at x=0.0 (0.8PMT-0.2PZT). The results of (0.8-y)PMT-yPT-0.2PMN (System II) and (0.8-z)PMT-zPT-0.2PZN (System III) were virtually identical to those of System I, but without any pyrochlore(s) even at y, z=0.0. Therefore, the introduction (20 mol%) of PZT and PZN (Systems I and III) turned out not to suppress the perovskite formation (except for x=0.0), although pyrochlore phases are prone to develop by the powder process in PZT [6–11] and PZN [6, 8, 14–17]. In addition, several peaks of the (pseudo)cubic perovskite at PMT-rich compositions became *noticeably* split with increasing values of x, y, and z in the three systems in common. Such phenomena, of course, resulted directly from the increasing fractions of PT of a tetragonal symmetry.

Table 1 Lattice parameters and tetragonality factors of a perovskite structure.

	Lattice parameter (nm)									Tetragonality factor		
	System I			System II			System III			I	II	III
x,y,z=	a	c	$(a^2c)^{1/3}$	a	c	$(a^2c)^{1/3}$	a	c	$(a^2c)^{1/3}$	c/a	c/a	c/a
0.8	0.39267	0.41123	0.39876	0.39356	0.41029	0.39906	0.39214	0.41400	0.39930	1.0473	1.0425	1.0557
0.6	0.39622	0.40615	0.39950	0.39499	0.40421	0.39804	0.39548	0.40760	0.39948	1.0251	1.0233	1.0307
0.4	0.39967	0.40316	0.40083	0.39681	0.40034	0.39798	0.39866	0.40416	0.40048	1.0087	1.0089	1.0138
0.2	0.40256		0.40256	0.40237		0.40237	0.40198		0.40198	1	1	1
0.0	0.40406		0.40406	0.40378		0.40378	0.40416		0.40416	1	1	1

The lattice parameters of the perovskite structure were determined and the results are listed in Table 1. Values of the lattice parameters (a, c, and $(a^2c)^{1/3}$) and the tetragonality factors (or axial ratios, c/a) of System I are plotted in Fig. 3. The crystallographic symmetries at x=0.0 and 0.2 (Fig. 2) are (pseudo)cubic, which became tetragonal with increasing PT fractions at x>0.2. Consequently, the values of a and c decreased and increased respectively at approximately similar rates, resulting in continuous increase in c/a to 1.0473 at x=0.8. At the same time, the average lattice parameters of $(a^2c)^{1/3}$ decreased steadily from 0.40406 to 0.39876 nm in the x=0.0–0.8 range, which is attributable to the gradual replacement of $Mg_{1/3}Ta_{2/3}$ by Ti, (weight-averaged) effective ionic radii of which are 0.0667 and 0.0605 nm [24], respectively. Variations of the lattice parameters and of the axial ratios in Systems II and III were similar to those of System I, except for a slight difference in values. Meanwhile, the poor sinterability of PT was successfully overcome by the introduction of 20 mol% substituents, which lead to the substantially lower values of c/a. The relative densities of the sintered ceramics were determined from measured and theoretical values (based on the perovskite lattice parameters), and the results were 93–95%, 92–97%, and 93–96% in the three systems.

Dependencies of the dielectric constant and loss (tanδ) values upon measurement frequency are presented in Fig. 4, but only for two representative compositions for simplicity. Typical relaxation behavior in the dielectric constant and loss was demonstrated at x=0.2, in which the maximum dielectric constant values decreased steadily as K_{max}= 18,100, 17,100, 16,000, and 14,600 at 1, 10, 100, and 1,000 kHz, respectively. In contrast, the dielectric maximum temperatures increased as T_{max}=16, 19, 22, and 26°C at the same frequency decades. Meanwhile, the magnitudes of the maximum dielectric loss and corresponding temperatures also increased with increasing frequency: 7.2% (−2°C), 8.9% (2°C), 11% (6°C), and 17% (12°C).

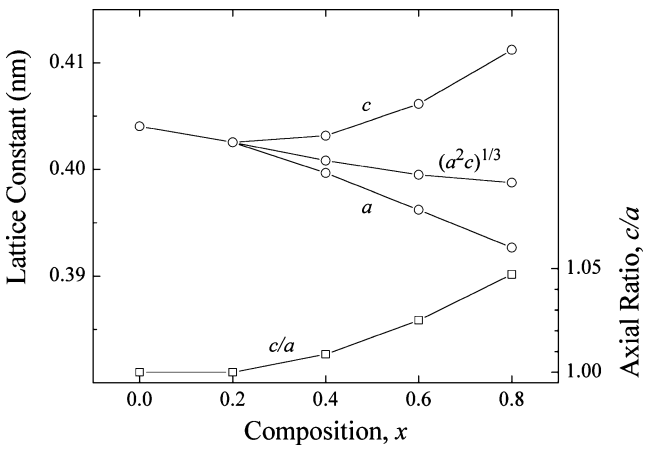

Fig. 3 Lattice parameters of a perovskite structure in System I

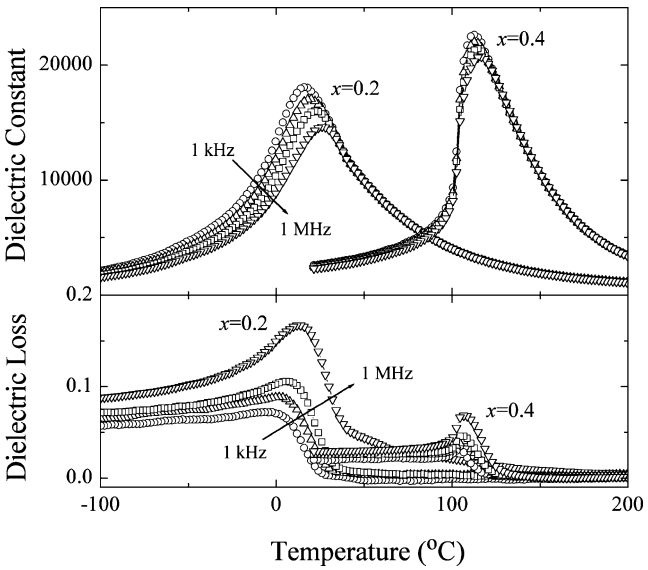

Fig. 4 Frequency-dependent dielectric constant and loss values of x= 0.2 and 0.4 (System I)

However, such frequency-dependent dispersion in the dielectric constant and loss was hardly observable in the adjacent composition of x=0.4.

The dielectric constant values of the three systems (1 kHz) are contrasted in Fig. 5 with compositional and temperature changes. The phase transition modes were quite diffuse at PMT-rich compositions of x,y,z=0.0 and 0.2, whereas the modes were comparatively sharp at x,z≥ 0.4 and y≥0.6. At the same time, the dielectric relaxation

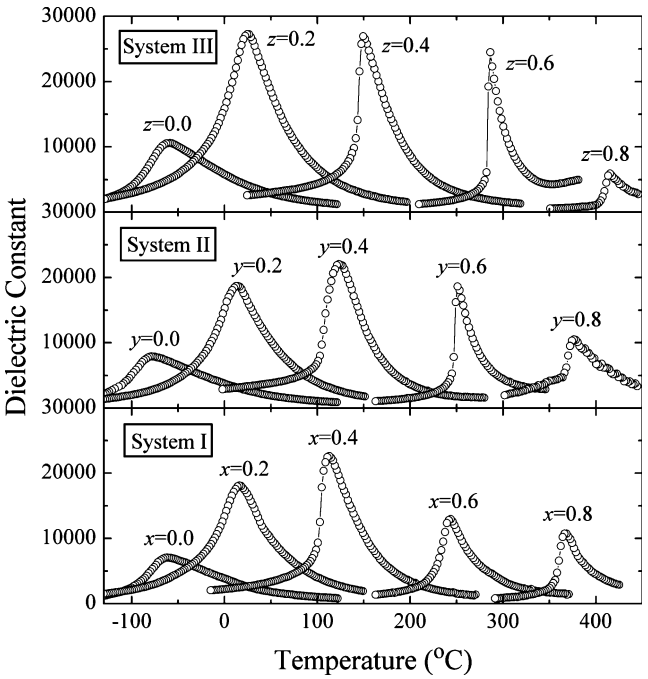

Fig. 5 Dielectric constant values of the ceramics in the three systems (1 kHz)

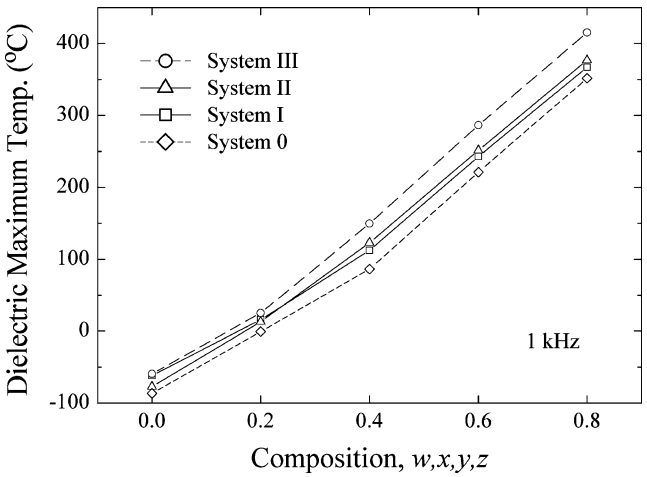

Fig. 6 Variations of the dielectric maximum temperature with compositional change. The data of (1-*w*)PMT-*w*PT (System 0) are also included for comparison

was appreciable at PMT-rich compositions, whereas such behavior was hardly observable at PT-rich compositions. However, the phase transition mode of y=0.4 was rather diffuse, but the frequency-dependent dispersion was minimal. Similar behavior of intermediate nature was also reported in $Pb(Fe_{1/2}Nb_{1/2})O_3$ and solid solutions thereof [25–27]. The gradual shifts from diffuse to sharp modes of phase transition in the three systems (regardless of the introduced species of PZT, PMN, and PZN) are interpreted to be closely associated with the compositional changes toward PT of sharp modes in the ferroelectric-paraelectric transition.

Meanwhile, the maximum dielectric constant values were highest at intermediate compositions in the three systems, similar to the variations in PMT-PT [5]. Among them, the values were highest in the case of PZN introduction (System III): K_{max}=27,300 (z=0.2) and 27,000 (z=0.4) at 1 kHz. The values were also very high in Systems I and II: 22,600 (x=0.4) and 22,100 (y=0.4). It is interesting to note that such high values were realized in System I with PZT incorporation. Such a positive role of PZT in promoting polarization is quite surprising, when the detrimental effects of the pyrochlore(s) on the dielectric properties [8, 18, 19] are considered. PZT has been well documented [6–11] to readily develop pyrochlore(s), instead of perovskite.

Variations of the dielectric maximum temperatures in the three systems are illustrated in Fig. 6, where the values of PMT-PT [5] are also included for comparison. The (1-*w*) PMT-*w*PT system is equivalent to (0.8-*w*)PMT-*w*PT-0.2PMT (i.e., (1-*w*)PMT-*w*PT with 20 mol% PMT introduction), which henceforth will be referred to as System 0. The T_{max} values increased continuously in general with increasing PT fractions: −86 to 352°C, −62 to 367°C, −77 to 377°C, and −59 to 415°C in the four systems, respectively. Hence, reduction of the wide T_{max} range in the PMT-PT system (−86–490°C) was accomplished somewhat by increasing and decreasing the temperatures at PMT- and PT-rich compositions.

It is interesting to note, however, that the variation modes of T_{max} can be classified into two major stages. In the first stage ($w,x,y,z \geq 0.4$), the increasing rates were virtually linear in the four systems. In contrast, the variations in the second stage (PMT-rich compositions of $w,x,y,z \leq 0.4$) were quite different and can be further classified into three groups. In the first (System 0) and third (System III) groups, the slopes changed rather abruptly at w=0.4 and z=0.2, respectively. In contrast, the transition points were intermediate (i.e., between those of w=0.4 and z=0.2) in the second group of Systems I and II. Such diversified T_{max}-X(composition) modes are currently interpreted to be related to the different cation species in the octahedral cage of the perovskite structure as follows. In Systems 0 and III, the numbers of the di-/penta-valent cations were identical: one each (Mg-Ta) in System 0 and two each (Mg/Zn-Ta/Nb) in System III, Eqs. 1 and 4. In Systems I and II, in contrast, the numbers of the octahedral cation species were two-one (Mg/Zn-Ta) and vice versa (Mg-Ta/Nb), Eqs. 2 and 3. Meanwhile, the presence of tetra-valent titanium in the four systems does not seem to play an important role. The cause of non-linearity in T_{max}-X in the range of $0.2 \leq x,y,z \leq 0.4$ is currently under investigation.

$$\text{System 0} : Pb\left[Mg_{(1-w)/3}Ti_wTa_{2(1-w)/3}\right]O_3, \quad (1)$$

$$\text{System I} : Pb\left[Mg_{(0.8-x)/3}Zn_{0.2/3}Ti_xTa_{2(1-x)/3}\right]O_3, \quad (2)$$

$$\text{System II} : Pb\left[Mg_{(1-y)/3}Ti_yTa_{2(0.8-y)/3}Nb_{0.4/3}\right]O_3, \quad (3)$$

$$\text{System III} : Pb\left[Mg_{(0.8-z)/3}Zn_{0.2/3}Ti_zTa_{2(0.8-z)/3}Nb_{0.4/3}\right]O_3 \quad (4)$$

In order to evaluate the phase transition modes, the dielectric constant values were further analyzed in terms of γ and C/K_{max}. The detailed physical meaning and numerical derivation methods have already been well reported in the literature [7, 9, 17, 28–30]. Dependencies of γ and C/K_{max} upon composition in the three systems are shown in Fig. 7, where magnitudes of the two parameters decreased in general with increasing x, y, and z. However, the decreasing modes in C/K_{max} were rather gradual in all of the three systems, whereas the modes were somewhat stepwise in γ. Nevertheless, the relative diffuseness/sharpness in the phase

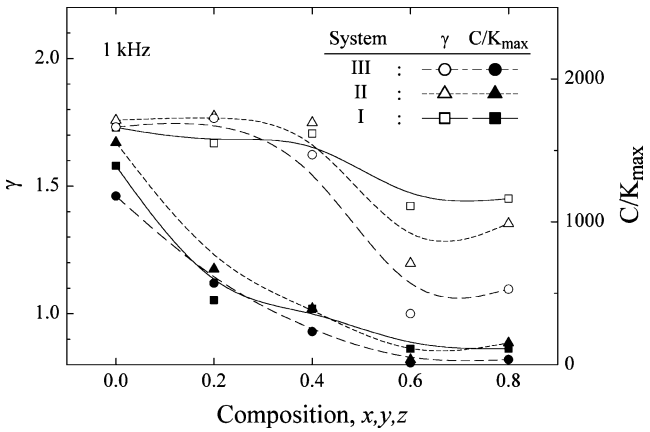

Fig. 7 Diffuseness parameters of γ and C/K_{max} in the three systems

transition modes of the dielectric constant values are well reflected in the variations of the two parameters.

The internal microstructures of selected composition ceramics (x=0.0, 0.2, and 0.4) are displayed in Fig. 8. The images of x=0.0 and 0.2 were composed mostly of multi-faceted perovskite with occasional pyrochlores scattered at the boundaries/junctions of the perovskite grains. The coexistence of the small-sized pyrochlore, however, was not observed in the XRD traces (Fig. 2), which is presumably due to the too small fractions for detection. Nevertheless, the lower values of the maximum dielectric constant at PMT-rich compositions in the three Systems (Fig. 5) seemed to have resulted from the coexisting pyrochlore. In contrast, only perovskite grains were present at x=0.4. The microstructures of the remaining compositions (x=0.6 and 0.8, and y,z=0.0–0.8 as well) were basically similar to those of x=0.4, except for somewhat different grain sizes. The entire fractomicrographs were generally consistent with the XRD results. Meanwhile, the observed fracture modes were preferentially intergranular in the investigated compositions, regardless of the presence of pyrochlore.

4 Summary

In the B-site precursor compositions, trirutile and columbite structures were only detected at x=0.0 (Zn-substituted case) and y=0.0 (Nb-substituted case), respectively, whereas the two structures coexisted at z=0.0 (simultaneous substitution by Zn and Nb). In contrast, only a rutile solid solution was identified at the opposite compositions of the three cases in common, which persisted down to x,y,z=0.4. At intermediate compositions of x,y,z=0.2, however, structures of trirutile+rutile, trirutile+columbite, and rutile+columbite coexisted in the precursor compositions of Systems I, II, III, respectively. After the additions of PbO into the precursor powders and proper calcination, only a perovskite structure resulted in all of the three systems, except for a negligible fraction of pyrochlore at x=0.0 (System I). In addition, (pseudo)cubic symmetries of the perovskite changed to tetragonal with increasing fractions of PT in the three systems, accompanying gradual increases in the axial ratio of c/a. The average lattice parameters of $(a^2c)^{1/3}$ also decreased steadily with increasing PT fractions.

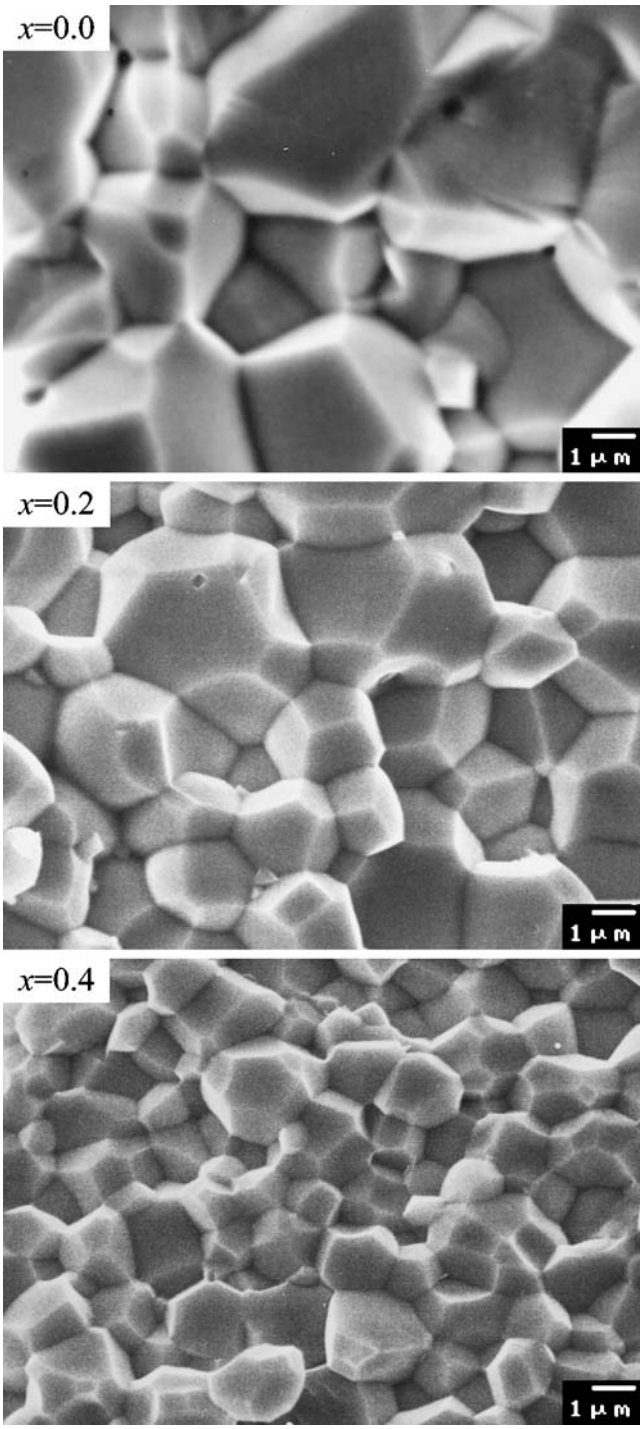

Fig. 8 Representative fractomicrographs of x=0.0, 0.2, and 0.4

Typical dielectric relaxation (with diffuse modes in the phase transition) was observed in PMT-rich ceramics (i.e., low values of x, y, and z), whereas the modes were rather sharp with little dispersion behavior at PT-rich compositions. Such changes in the phase transition modes were also verified numerically by separate analysis in terms of the diffuseness parameters (γ and C/K_{max}). The maximum dielectric constant values were higher at intermediate compositions in the three systems, but the dielectric maximum temperatures increased steadily with increasing fractions of PT. However, apparent changes in the slopes of the T_{max}-X relations were observed at w=0.4 (Systems 0) and z=0.2 (System III), whereas the changes were rather gradual in Systems I and II. The fractomicrographs of the ceramics consisted basically of multi-faceted perovskite grains (except for the additional pyrochlore(s) at PMT-rich compositions) with preferential fracture modes of the intergranular-type.

Acknowledgment This study was supported by the Korea Research Foundation Grant (KRF-2001-041-E00456).

References

1. V.A. Bokov, I.E. Myl'nikova, Sov. Phys., Solid State **2**(11), 2428 (1961)
2. A.A. Bokov, Z.-G. Ye, Solid State Commun. **116**(2), 105 (2000)
3. I.W. Chen, J. Phys. Chem. Solids **61**(2), 197 (2000)
4. B.A. Malkov, Yu.N. Venevtsev, Inorg. Mater. **13**(8), 1189 (1977)
5. J.-S. Kim, N.-K. Kim, Mater. Res. Bull. **35**(14–15), 2479 (2000)
6. H.C. Ling, M.F. Yan, W.W. Rhodes, Ferroelectrics **89**, 69 (1989)
7. S.-M. Lim, N.-K. Kim, J. Mater. Sci. **35**(17), 4373 (2000)
8. T.R. Shrout, A. Halliyal, Am. Ceram. Soc. Bull. **66**(4), 704 (1987)
9. M.-C. Chae, S.-M. Lim, N.-K. Kim, Ferroelectrics **242**(1–4), 25 (2000)
10. B.-Y. Ahn, N.-K. Kim, Mater. Res. Bull. **35**(10), 1677 (2000)
11. J.-S. Kim, N.-K. Kim, H. Kim, J. Am. Ceram. Soc. **86**(6), 929 (2003)
12. Y.J. Kim, S.W. Choi, Ferroelectrics **108**, 241 (1990)
13. S.W. Choi, J.M. Jung, J. Kor. Phys. Soc. **29**(Suppl.), S672 (1996)
14. D.-H. Lee, N.-K. Kim, Mater. Lett. **34**(3–6), 299 (1998)
15. M.-C. Chae, N.-K. Kim, J.-J. Kim, S.-H. Cho, J. Mater. Sci. **33**(5), 1343 (1998)
16. M.-C. Chae, N.-K. Kim, J.-J. Kim, S.-H. Cho, Ferroelectrics **211** (1–4), 25 (1998)
17. B.-Y. Ahn, N.-K. Kim, J. Am. Ceram. Soc. **83**(7), 1720 (2000)
18. J. Chen, A. Gorton, H.M. Chan, M.P. Harmer, J. Am. Ceram. Soc. **69**(12), C303 (1986)
19. M.F. Yan, H.C. Ling, W.W. Rhodes, J. Mater. Res. **4**(4), 930 (1989)
20. B.-H. Lee, N.-K. Kim, J.-J. Kim, S.-H. Cho, Ferroelectrics **211**(1–4), 233 (1998)
21. S. Ananta, N.W. Thomas, J. Eur. Ceram. Soc. **19**(2), 155 (1999)
22. S.L. Swartz, T.R. Shrout, Mater. Res. Bull. **17**(10), 1245 (1982)
23. S.L. Swartz, T.R. Shrout, W.A. Schulze, L.E. Cross, J. Am. Ceram. Soc. **67**(5), 311 (1984)
24. R.D. Shannon, Acta Crystallogr. **A32**(5), 751 (1976)
25. M. Yokosuka, Jpn. J. Appl. Phys. **38**(9B), 5488 (1999)
26. X.S. Gao, X.Y. Chen, J. Yin, J. Wu, Z.G. Liu, M. Wang, J. Mater. Sci. **35**(21), 5421 (2000)
27. B.-C. Woo, B.-K. Kim, J.-H. Lee, H.-M. Park, B.H. Kim, J. Kor. Ceram. Soc. **39**(9), 863 (2002)
28. K. Uchino, S. Nomura, Ferroelectr. Lett. **44**(3), 55 (1982)
29. S.J. Butcher, N.W. Thomas, J. Phys. Chem. Solids **52**(4), 595 (1991)
30. M. Kuwabara, S. Takahashi, K. Goda, K. Oshima, K. Watanabe, Jpn. J. Appl. Phys. **31**(9B), 3241 (1992)